EUROFUSION WPMST1-PR(16) 15380

WA Suttrop et al.

Progress in understanding the plasma response to non-axisymmetric magnetic perturbations in tokamaks

Preprint of Paper to be submitted for publication in
43rd European Physical Society Conference on Plasma Physics (EPS)

This work has been carried out within the framework of the EUROfusion Consortium and has received funding from the Euratom research and training programme 2014-2018 under grant agreement No 633053. The views and opinions expressed herein do not necessarily reflect those of the European Commission.

Experimental studies of high-confinement mode plasma response to non-axisymmetric magnetic perturbations in ASDEX Upgrade

W Suttrop[1], A Kirk[2], R Nazikian[3], N Leuthold[1], E Strumberger[1], M Willensdorfer[1], M Cavedon[1], M Dunne[1], R Fischer[1], S Fietz[1], J C Fuchs[1], Y Q Liu[2], R M McDermott[1], F Orain[1], D A Ryan[2,4], E Viezzer[1], the ASDEX Upgrade Team, the DIII-D Team and the Eurofusion MST1 Team[5]

[1]Max-Planck-Institut für Plasmaphysik, D-85740 Garching, Germany
[2]CCFE, Culham Science Centre, Abingdon, Oxon, OX14 3DB, U.K.
[3]Princeton Plasma Physics Laboratory, PO Box 451, Princeton, New Jersey 08543-0451, U.S.A.
[4]Department of Physics, University of York, YO10 5DD, York, U.K.
[5]see `http://www.euro-fusionscipub.org/mst1`

E-mail: `Wolfgang.Suttrop@ipp.mpg.de`

Abstract. The interaction of externally applied small non-axisymmetric magnetic perturbations (MP) with tokamak high-confinement mode (H-mode) plasmas is reviewed and illustrated by recent experiments in ASDEX Upgrade. The plasma response to the vacuum MP field is amplified by stable ideal kink modes with low toroidal mode number n driven by the H-mode edge pressure gradient (and associated bootstrap current) which is experimentally evidenced by an observable shift of the poloidal mode number m away from field alignment ($m = qn$, with q being the safety factor) at the response maximum. A torque scan experiment demonstrates the importance of the perpendicular electron flow for shielding of the resonant magnetic perturbation, as expected from a two-fluid MHD picture. Two significant effects of MP occur in H-mode plasmas at low pedestal collisionality, $\nu^*_{\rm ped} \leq 0.4$: (a) a reduction of the global plasma density by up to 50% and (b) a reduction of the energy loss associated with edge localised modes (ELMs) by a factor of up to 10. A comprehensive database of ELM mitigation pulses at low ν^* in ASDEX Upgrade shows that the degree of ELM mitigation correlates with the reduction of pedestal pressure which in turn is limited and defined by the onset of ELMs, i. e. a modification of the ELM stability limit by the magnetic perturbation.

PACS numbers: 52.55.Fa, 52.55.Tn, 52.65.Kj

1. Introduction

Deviations from the nominally axisymmetric toroidal magnetic configuration of tokamaks, both by plasma internal helical modes and by static error fields [1], are a concern because they can compromise device performance in various ways. Collisionless ("ripple") particle losses, especially those of energetic alpha particles in a reactor [2] may concentrate excessive power density onto small wall areas [3]. Unintended field errors can be of various origin such as tolerances in the mounting positions of toroidal and poloidal field coils, localised supply current feeds of magnetic field coils, non-axisymmetric ferromagnets, and (on a low level) the earth magnetic field. Detrimental effects of field errors can be reduced by compensating non-axisymmetric fields from suitably designed sets of actively driven correction coils [4], which have been implemented for a range of contemporary tokamaks [5, 6, 7, 8, 9, 10]. If a magnetic perturbation (MP) is *resonant* with the plasma, i.e. Fourier components with toroidal mode number n and poloidal mode number m align with the safety factor $q(r)$ such that $q = m/n$, nested flux surfaces break up and magnetic islands form. The interaction of island chains with different m/n leads to various degrees of stochasticity, i.e. radial diffusion of magnetic field lines and a dissolution of local order [11, 12]. Fast radial transport parallel to the magnetic field [13, 14] leads to a reduction of the pressure gradient and thereby a reduction of tokamak confinement. The magnetic field topology change by MPs has been used to produce "ergodic divertor" configurations with significant parallel connection length between closed flux surfaces and the plasma-facing wall in Tore Supra [15] and TEXTOR-DED [16] which is advantageous compared to the limiter configuration used otherwise in these tokamaks.

Magnetic perturbations can also be purposely applied to control performance limiting MHD instabilities [17] and increase the attainable plasma beta (average kinetic pressure, normalised to central magnetic field pressure). The amplification of the external MP by stable modes is useful to diagnose the damping rate especially above the no-wall beta-limit where kinetic resonances can become important [18, 19, 20]. The Resistive Wall Mode (RWM, [21]) is particularly amenable for feed-back controlled stabilisation because its growth rate is controlled by the resistivity of the surrounding wall and can be adjusted to be within the bandwidth of the feedback system. In situations where the RWM imposes the beta limit, a significant increase of plasma beta has been achieved by RWM control in tokamaks [22, 23]. In reversed-field-pinches (RFP) multiple unstable modes are stabilised simultaneously by using elaborate feedback systems with a large number of sensors and actuator coils [24, 25] leading to significant performance improvements and the possibility to retain in a so-called "quasi single-helicity" mode essentially only one island chain needed to produce the toroidal field reversal required for the RFP configuration [26]. Recent advances in the field of high-beta MHD stability limits are presented in a separate paper in this issue [27] and are not further discussed here.

A second main application of non-axisymmetric magnetic perturbations in tokamaks, and the main subject of this paper, is to control the Edge Localised Mode (ELM) instability [28, 29, 30]. It is driven by the edge pressure gradient and associated bootstrap current [31] in the edge transport barrier in High-confinement Mode (H-mode) and causes repetitive outbursts of plasma energy and particles. Shortly after the discovery of H-mode [32] the possibility of ELM mitigation by magnetic perturbations was observed [33, 34]. The effect of the MP is to reduce the ELM energy loss from the main plasma, and thereby the peak heat load onto the surrounding wall with the side effect of increasing the repetition frequency of ELMs. ELM mitigation by magnetic perturbations is now a robust observation [35] which has been reproduced and studied in a variety of tokamaks [36, 37, 38, 39, 40, 41]. The possibility to eliminate ELM bursts altogether by MPs in favour of quiescent stationary H-mode plasmas has been discovered in experiments in DIII-D [42, 43] and has later been reproduced in KSTAR [44] and very recently in ASDEX Upgrade (see below). As long as predictions of ELM losses are uncertain, suppression of ELMs may be the safest option to meet ITER's challenging limitations for transient first wall heat loads [45]. An in-vessel coil set has been designed for ITER that mimics the ones in DIII-D, KSTAR and ASDEX Upgrade but offers more control over the toroidal and poloidal mode spectrum [46].

In parallel with the experimental progress, the understanding of the plasma response to the external magnetic perturbation has evolved in the recent years. A large body of work has been performed to study experimentally the modifications introduced by magnetic perturbations to limiter plasmas [47] and poloidal divertors [48]. Ignoring non-axisymmetric response currents in the plasma the total magnetic field can be described in the so-called "vacuum approximation" by a superposition of the fields of the axisymmetric unperturbed force equilibrium and the vacuum field produced by the perturbation coils. The vacuum approximation works well if plasma response currents are weak, e.g. in the cold scrape-off-layer [48]. However, in response to the external perturbation field, the plasma often produces field-aligned non-axisymmetric response currents, for example thermo-electrical currents [49] or currents induced by plasma flows across the magnetic field [50], which are usually directed such that the associated field is opposite to the vacuum field inside the flow region and therefore the resonant MP is shielded from the plasma core. Because of strong flows and low resistivity this shielding effect is substantial in H-mode plasmas and will normally lead to suppression of islands and restoration of intact flux surfaces already within the narrow edge gradient region [51]. From two-fluid MHD [52, 50, 53, 54] the perpendicular electron flow rather than the fluid (mass) velocity is expected to control field shielding, which is demonstrated in a seminal experiment in TEXTOR that finds a minimum threshold for field penetration if the difference of electron perpendicular flow and magnetic perturbation rotation speed is minimised [55]. The electron perpendicular flow is always very strong (in electron drift direction) in the H-mode edge transport barrier because of the strong negative (inward-directed) radial electrical field and the strong electron diamagnetic flow [50], hence the gradient region is in practice always shielding resonant field components very well. In poloidal divertor geometry the safety factor diverges towards the separatrix and there are typically many closely spaced resonant surfaces near the plasma edge. Despite the large global shear the local shear near the outer midplane is usually small in the gradient region of typical H-mode pulses. Hence for MP coils mounted close to the plasma at the outer midplane the field-alignment condition is usually fulfilled for all (or no) resonant surfaces in the gradient region simultaneously, which allows to select experimentally whether to couple to shielded (resonant) or unshielded (non-resonant) modes [56].

The magnetic perturbation can also be amplified, both by ideal and resistive types of plasma response [57]. Resistive response can originate from any process that drives tearing-unstable plasma current profiles [34] or the reduction of bootstrap current in the interior of already existing magnetic islands ("neoclassical tearing"). These processes are typically non-linear which is experimentally observed as threshold behaviour for the onset of field amplification, often dubbed "field penetration" [58]. The presence of a strong edge pressure gradient in H-mode gives rise to MP amplification by an ideal kink response [59, 60, 53, 61] in analogy to the beta-driven resonant field amplification in the core but by coupling to stable eigenmodes that are radially localised to the gradient region and its near vicinity. An amplification of plasma displacement above that expected in the vacuum approximation is indeed observed in DIII-D [62, 63], ASDEX Upgrade [64], JET, NSTX and MAST [65]. Poloidal mode coupling due to toroidicity and plasma elongation causes the most strongly responding modes (least stable eigenmodes) to contain resonant components [61, 66]. As a consequence, excitation of unshielded non-resonant components by the MP field will cause deformations that locally produce resonant fields which can possibly produce topology changes even inside the shielding layer in the edge gradient region. Recent simulations of an ELM mitigation scenario in ASDEX Upgrade with the non-linear, resistive MHD code JOREK [67] suggest that resistive effects due to this mode coupling are particularly pronounced near the X-point region as has been found before in linear MARS-F calculations [60]. The consequences of these findings for ELM mitigation and ELM suppression, however, are still a matter of ongoing research.

In this paper, we focus on ELM mitigation and ELM suppression at low edge collisionality and examine in which way the plasma response in these H-mode regimes appears in experimental practice. We mainly consider experiments in ASDEX Upgrade, which has been retrofitted with a versatile set of in-vessel saddle coils [68] with independent power supplies [69] that allow for a flexible perturbation field structure. ELM mitigation at low [41] and high pedestal collisionality [38, 56] as well as ELM suppression scenarios are accessible and studied intensively in ASDEX Upgrade. This paper is organised as follows. We first review the effects of magnetic perturbations on H-mode plasmas and concentrate on regimes at low pedestal collisionality. We then discuss an experimental scan of magnetic perturbation field structure which demonstrates the importance of the edge kink response for ELM mitigation. The plasma flow is varied by a dedicated torque scan experiment which demonstrates the field shielding effect in H-mode, complementing the TEXTOR result which was obtained in L-mode. We conclude with a discussion of our results and implications for further investigation.

2. ELM mitigation and ELM suppression

We first inspect the phenomenology of ELM mitigation and ELM suppression by magnetic perturbations using examples from recent experiments in ASDEX Upgrade. Both regimes are obtained reproducibly in very similar H-mode plasmas. The plasma cross section of two example pulses is shown in figure 1 along with sightlines of some essential diagnostics and the position of upper and lower in-vessel coil rows, dubbed “Bu” and “Bl”, respectively. Pulse 31128 (ELM mitigation) is a low triangularity configuration (upper and lower triangularity: $\delta_u = 0.05$, $\delta_l = 0.43$, elongation: $\kappa = 1.63$), whereas pulse 33353 (ELM suppression) has increased upper triangularity ($\delta_u = 0.23$) while the other shaping parameters are similar ($\delta_l = 0.42$, $\kappa = 1.65$). Stronger plasma shaping is found essential to achieve ELM suppression, as well the precise value of the edge safety factor. For pulse 33353, $q_{95} = 3.65$, below a critical value of $q_{95} = 3.7$, above which only ELM mitigation is obtained, but not full suppression of ELMs. For the ELM mitigation pulse 31128, $q_{95} = 3.8$. Because of the different plasma shape, keeping q_{95} similar implies different plasma current in both discharges, namely $I_p = 0.885$ MA and $I_p = 0.8$ MA, respectively.

Figure 2 shows time traces for both shots during the H-mode plasma current flat top. Both discharges use very similar heating, 6 MW neutral beam power and $2.5-3$ MW centrally deposited ECRH power (frequency 140 GHz) in third harmonic X-mode. The toroidal field $B_t = -1.8$ T is selected such that the second harmonic is also absorbed within the plasma

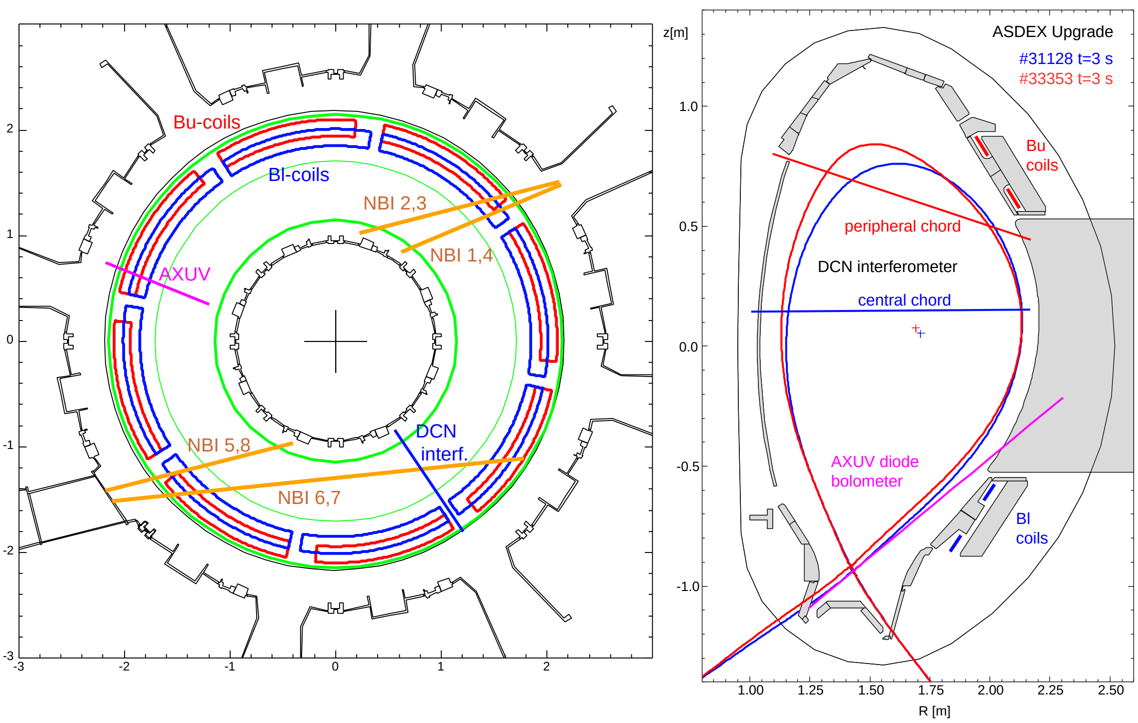

Figure 1. Left: Top view, Right: Poloidal cross section of ASDEX Upgrade with NBI geometry, location of upper (“Bu”) and lower (“Bl”) magnetic perturbation coils, locations of selected diagnostics and plasma shapes for discharges 31128 and 33353

at a resonance on the high field side to effectively act as a beam dump for any radiation unabsorbed at the X3 resonance [70]. ASDEX Upgrade is equipped with a fully tungsten cladded wall, and central ECRH is essential to maintain peaked electron temperature profiles to ensure outward transport of tungsten impurities in the plasma core to avoid accumulation and a radiative collapse [71] especially for these low density H-mode discharges. Soon after stable ELMy H-mode is set up, the gas puff is switched off (pulse 31128) or reduced to a very low level of 10^{21} D/s (pulse 33353) and the magnetic perturbation is switched on. In both cases an identical MP configuration is used with toroidal mode number $n = 2$, maximum DC MP coil current $I_{\mathrm{MP}} = 1.3$ kA and a relative phase offset of the upper coil ring relative to the lower ring of $\Delta\Phi = +90°$. This results in essentially identical mode number spectra for the two shots. A short reference phase without ELM mitigation in the case of low shaping at low density exists in shot 31128 for $t = 2.0 - 2.5$ s, before the MP is switched on. With stronger shaping such as in shot 33353, the ELM frequency (without MP) becomes low so that the tungsten influx in between ELMs is sufficient to reach accumulation and a radiative collapse, which takes the form of a very big ELM and back-transition to L-mode. For this reason, the MP is applied well before the gas feed is reduced, thereby keeping up a sufficiently large ELM frequency to avoid radiative collapse. ELM mitigation becomes effective in pulse 31128 after $t = 2.6$ s (Figure 2 a) and takes the form of a gradual reduction of ELM losses, peak divertor

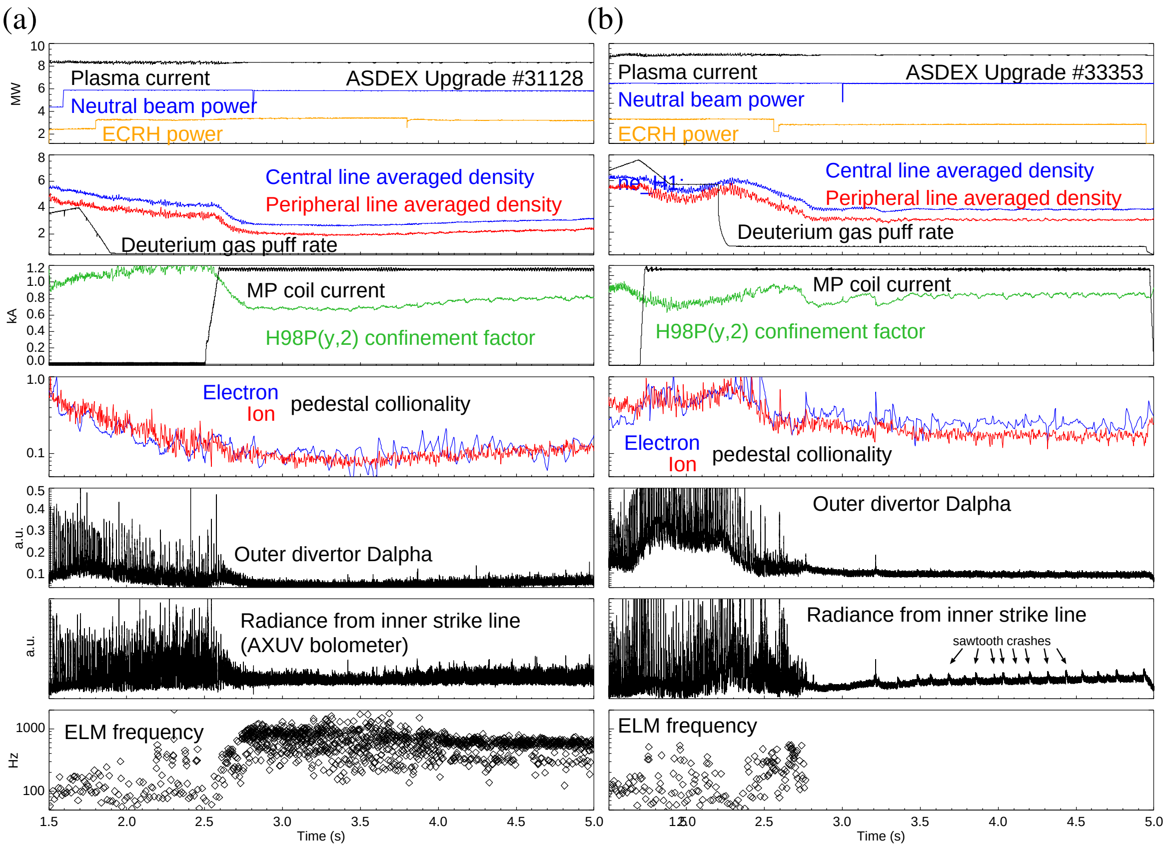

Figure 2. Time traces of H-mode discharges in ASDEX Upgrade showing (a) ELM mitigation and (b) ELM suppression by magnetic perturbations.

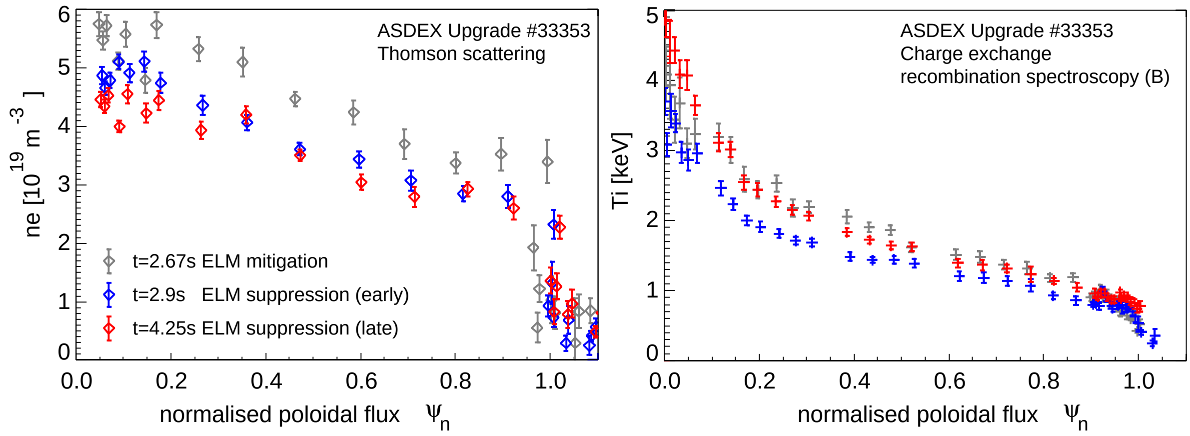

Figure 3. Profiles of electron density (left) and ion temperature (right) before and during ELM suppression in shot 33353

recycling as measured by the D_α intensity and a gradual increase of ELM frequency. The radiation originating from the inner divertor strike zone measured by AXUV bolometer diodes is particularly sensitive even to detect small ELMs, and in this phase small ELM crashes are detected. In pulse 33353 (Figure 2 b), ELM suppression is reached at $t = 2.75$ s, after a rapid transition from a preceding phase with various degrees of ELM mitigation. The decisive trigger appears to be the reduction of the plasma density and the pedestal electron and ion collisionalities (to below $\nu^*_{\mathrm{ped,e,i}} \sim 0.25$, using the definition in [72]) after the gas puff is reduced. Except for one event at $t = 3.2$ s, there is no indication of ELM crashes in midplane and divertor signals any longer. After $t = 3.2$ s small repetitive peaks in the divertor D_α are found, which are correlated with the arrival of sawtooth crash pressure pulses at the plasma edge. The absence of short-time broadband bursts in the magnetic signals suggests that no ELM is triggered by these sawtooth crashes. In both cases, a strong density reduction occurs as the MP is switched on, most strongly seen in the case of shot 31128 without gas puff at that time. Consequently the confinement, measured here by the ITER IPB-$H_{98Py,2}$ confinement factor [73], drops in the ELM mitigated or ELM suppressed phases compared to phases with MP off, however in the ELM suppressed case it recovers from an initial $H_{98Py,2} = 0.8$ after the transition to ELM suppression back to $H_{98Py,2} = 0.95$, comparable with the confinement level during ELM mitigation ($t = 2.5 - 2.75$ s). Figure 3 shows electron density and ion temperature profiles of this discharge shortly before the transition to ELM suppression ($t = 2.67$ s), shortly afterwards ($t = 2.9$ s) and at a later time where $H_{98Py,2}$ has recovered. While the density drop associated with ELM suppression persists, the ion temperature recovers approximately to its original value before the transition. The electron temperature (not shown) shows much weaker variation.

ELM suppression is a new finding in ASDEX Upgrade and to date only a few discharges have been made, leaving open the question of how far this scenario can potentially be optimised. A much larger database exists for ELM mitigation in ASDEX Upgrade at varying pedestal collisionality, with plasma shapes similar to that of shot 31128 (low triangularity)

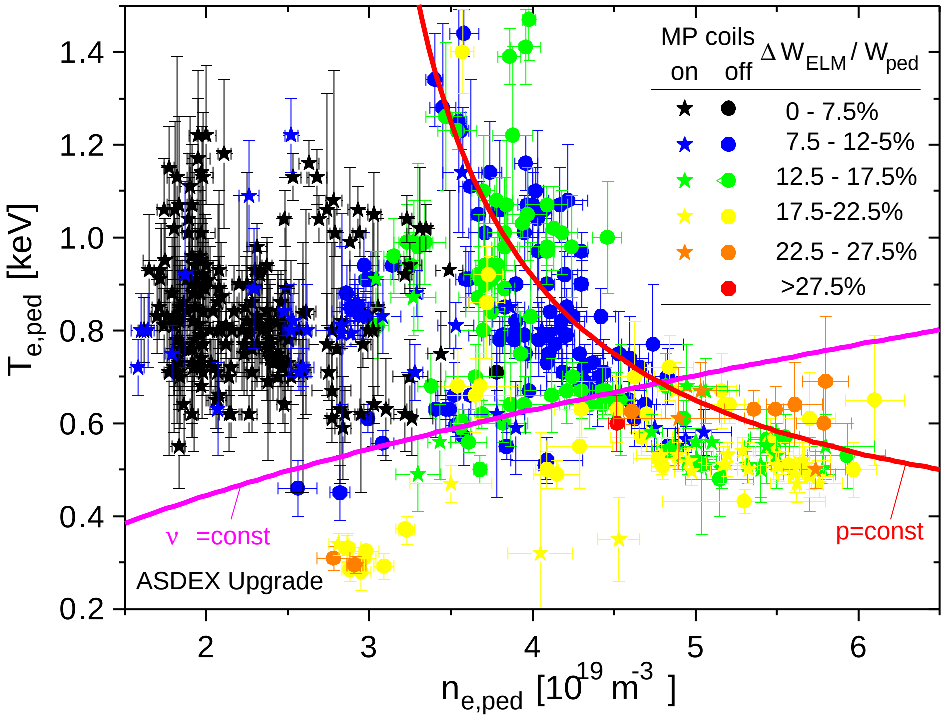

Figure 4. ELM losses $\Delta W_{\mathrm{ELM}}/W_{\mathrm{ped}}$ with MP on (asterisks) and off (circles) in pedestal $T_e - n_e$ space

and at varying safety factor. This database is used in a recent study to examine the pedestal parameter dependence of the degree of ELM mitigation [74]. Figure 4 shows the ELM energy loss ΔW_{ELM}, normalised to the pedestal stored energy $W_{\mathrm{ped}} = 3/2 p_{\mathrm{ped}} V$ (V: plasma volume), for a large set of time intervals in pedestal $T_e - n_e$ space, a representation similar to that introduced in [75]. Values of T_e and n_e are taken at the intersection of linear fits to profiles in the gradient region and the pedestal top region. Curves of constant pressure and collisionality are added to the figure. The largest ELMs are found at highest pedestal pressure, in-line with the ideal pressure limit imposed by type I ELMs on the pedestal. Phases with strong ELM mitigation by MP populate a region at low density and reduced pedestal pressure below a collisionality threshold which, without MP, is typically the locus of ELM free H-mode in ASDEX Upgrade [75]. High temperature forms of small ELMs populating this area in edge operational space have been observed before in DIII-D [76], JET [77] and MAST [78] albeit without explicit application of MPs.

It might be suspected that the ELM size is a mere function of pedestal pressure and collisionality and that the ELM mitigation effect of the magnetic perturbation comes in solely by the reduction of density. This can be studied by separating the time scales of the MP field variation and the density pump-out. In ASDEX Upgrade, the MP coils are mounted on a massive copper conductor ("passive stabilisation loop", PSL) which is used to reduce the vertical growth rate, but which also partially shields fast MP transients produced by the MP coils. Figure 5 shows time traces of an experiment in which the MP is switched off quickly (within 10 ms, at $t = 2.5$ s) using an MP coil current trajectory which is designed to

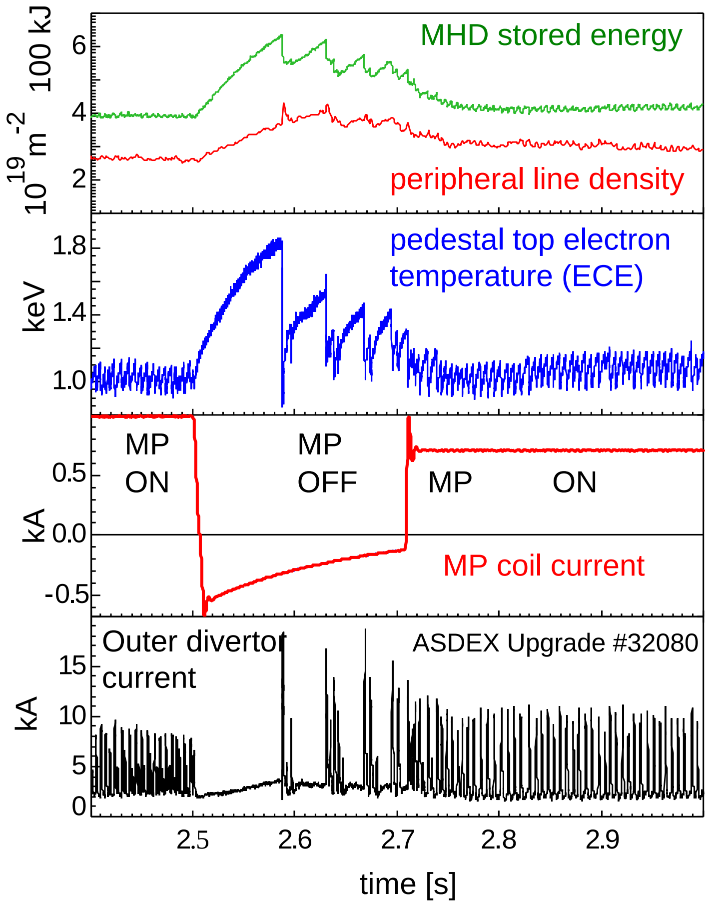

Figure 5. Time traces of an experiment to separate density recovery and MP turn-off time scales, showing that maintaining continuous mitigated ELM activity requires the presence of the MP.

compensate the field at the plasma surface produced by the image currents in the PSL. The mitigated ELMs observed in the phase before disappear immediately and an ELM-free phase is encountered during which the pedestal density and temperature increase until, at much larger pedestal pressure than with MP on, a sequence of large ELMs occurs. ELM mitigation is recovered at $t = 2.7$ s when the MP coils are switched on again. However, immediately after switching off the MP at $t = 2.5$ s, there are no ELMs at all despite the pedestal density and pressure being still near their values in the preceding phase with MP on and mitigated ELM activity. This finding demonstrates that with very similar pedestal parameters, the existence of ELMs depends explicitly on the presence of the MP. In other words, non-axisymmetry of the magnetic field is necessary to render the small ELMs unstable while the edge pressure is below that of type I ELMs. It is noteworthy that MP is not the only way to destabilise ELMs in this parameter regime, as for example type-IV ELMs in MAST have been obtained by modifications of the fuelling arrangement [78].

3. Effect of magnetic perturbation spectrum

The reaction of ELMs and plasma density to magnetic perturbations depends critically on the structure of the applied perturbation field. Fig. 6 shows time traces of two discharges similar to pulse 31128 (Fig. 2 a) except for the differential phase $\Delta\Phi$ between the $n = 2$ current pattern in upper and lower coil rings which is continuously varied. The plasma response is measured by the degree of ELM mitigation (reduction of divertor power, ELM frequency increase) and by the magnitude of density pump-out with no-MP reference values indicated by the dashed lines. The plasma response is maximised in the range of $\Delta\Phi = 90° - 150°$, well offset from $\Delta\Phi = 30°$ which corresponds to alignment of the MP with the plasma edge magnetic field. It is interesting to note that at $\Delta\Phi \approx -90°$, classical ELM free phases are triggered at $t = 2.85$ s (30682) and $t = 3.0$ s (30826), which lead to an accumulation of density and increase of impurity radiation. Once triggered, the intrinsic transport dynamics of the ELM-free phase overlays the effect of the $\Delta\Phi$ ramp, and if $\Delta\Phi$ is held constant (as in 30682) it is self-terminating by big ELM activity and a collapse of the edge pedestal.

It is instructive to compare the vacuum and ideal plasma responses for the extreme cases, $\Delta\Phi = +90°$ (optimum response and ELM mitigation) and $\Delta\Phi = -90°$ (ELM-free trigger). The plasma response is approximated here by the three-dimensional ideal MHD equilibrium for the low triangularity case (shots 31128, 30682 and 30826) which is calculated with the NEMEC code as described in Refs. [79, 80], starting from a kinetically constrained axisymmetric free-boundary equilibrium and the vacuum perturbation field for each $\Delta\Phi$. In Figure 7 the normal field amplitude of $n = 2$ modes is plotted as a function of poloidal mode number m and normalised poloidal flux ψ_n as radial coordinate for the cases of strongest

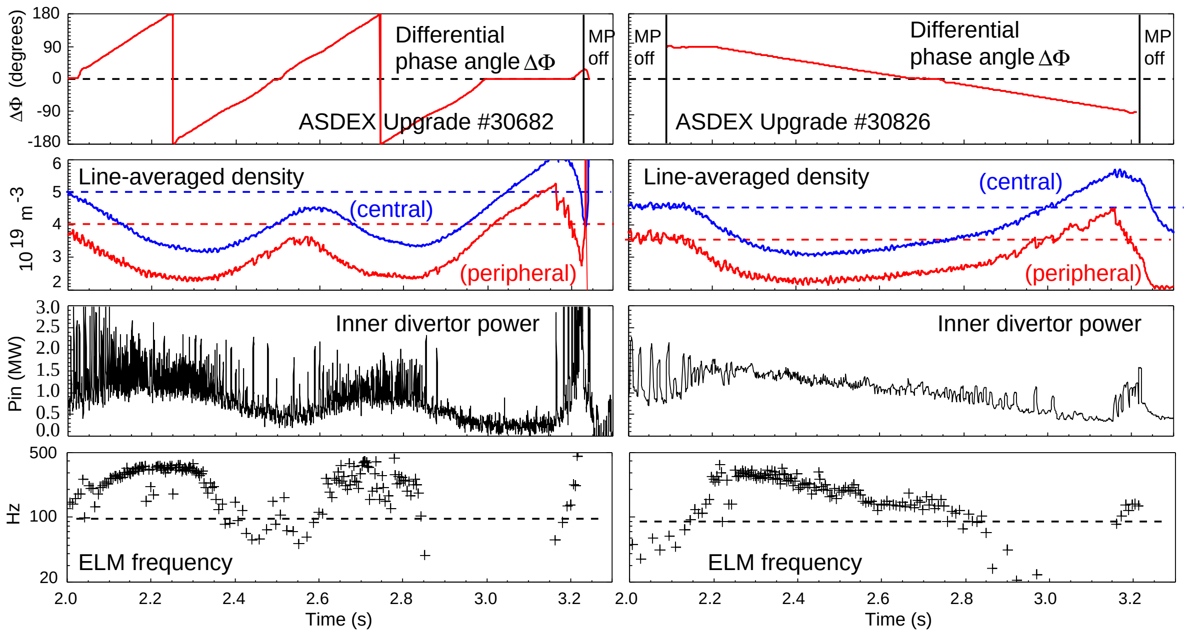

Figure 6. Time traces of shot 30682 (left) and shot 30826 (right) with $n = 2$ magnetic perturbation and continuously varied differential phase $\Delta\Phi$ between upper and lower coil rings.

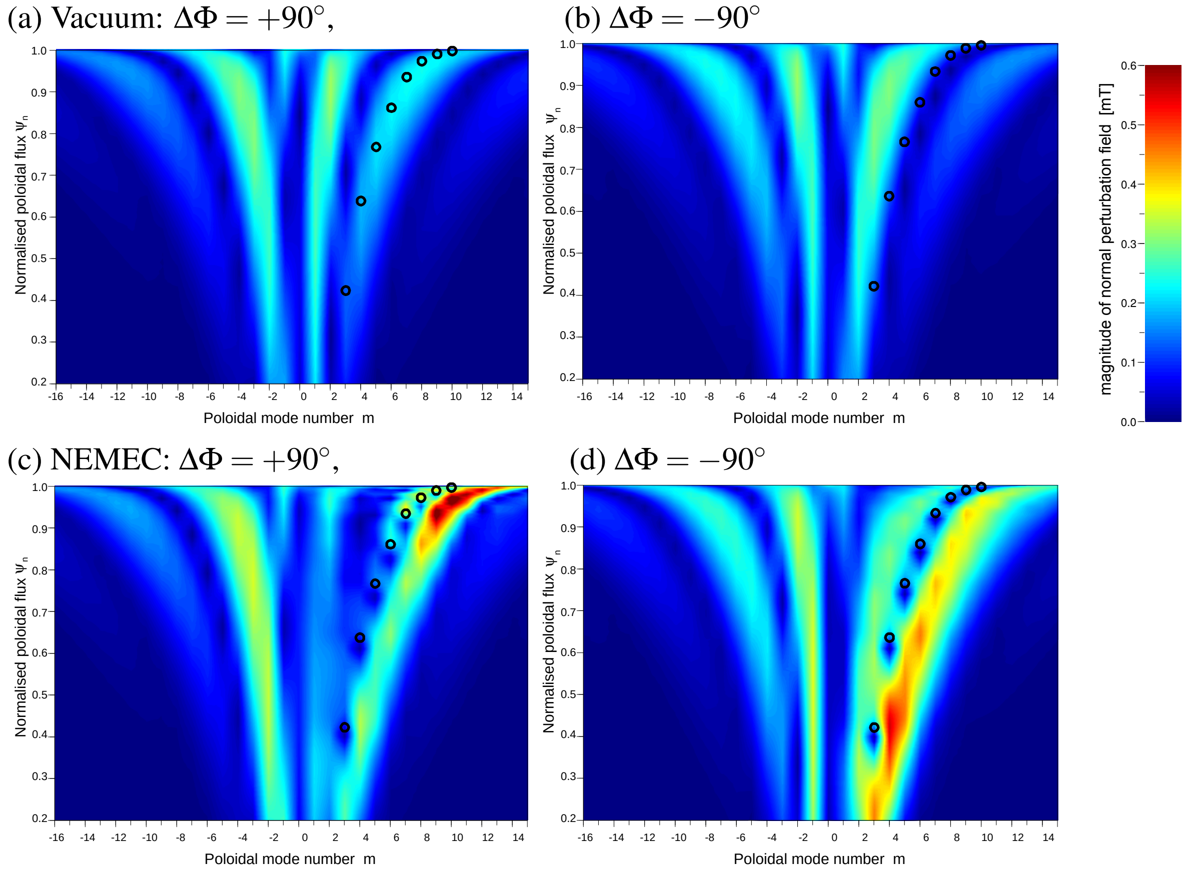

Figure 7. Poloidal spectrum of the normal perturbation field ($n = 2$) in vacuum (a, b) and as calculated by NEMEC (c, d) for $\Delta\Phi = +90°$ (maximum response; a, c) and $\Delta\Phi = -90°$ (ELM-free trigger; b, d) as a function of normalised poloidal flux. The black circles correspond to rational surfaces.

ELM mitigation, $\Delta\Phi = +90°$ (a, b), and onset of ELM-free phases, $\Delta\Phi = -90°$ (c, d). In all figures, the resonant $m = q(\psi_n) \cdot n$ on rational surfaces (half-integer q) is over-plotted as black circles. The vacuum field is moderately resonant with the plasma for $\Delta\Phi = +90°$ and mostly non-resonant for $\Delta\Phi = -90°$ (Figure 7 a, b). In the NEMEC solution (Figure 7 c, d), the resonant field components are strongly reduced and essentially suppressed just inside resonant surfaces. This is an effect of implicit sheet currents in the NEMEC solution which ensure intact nested flux surface topology in the 3D equilibrium. The plasma response leads to strong enhancement of non-resonant components at $m = q \cdot n + 2$ which are localised near the edge gradient region at $\psi_n > 0.9$ for $\Delta\Phi = +90°$ and are global with a peak in the plasma core for $\Delta\Phi = -90°$. These components are driven by the edge pressure gradient and the core pressure gradient, respectively. A poloidal cross section of the field produced by helical plasma currents in response to the MP (i.e. vacuum field subtracted) is shown in Fig. 8. The strongly edge-localised MP amplification ($\Delta\Phi = +90°$, Fig. 8 a) is also concentrated at the plasma top and near the X-point while the core MP response ($\Delta\Phi = -90°$, Fig. 8 b) is strongest around the low field side mid-plane. Both radial and poloidal localisation of the amplifying plasma response for the various values of $\Delta\Phi$ agree fully with the results

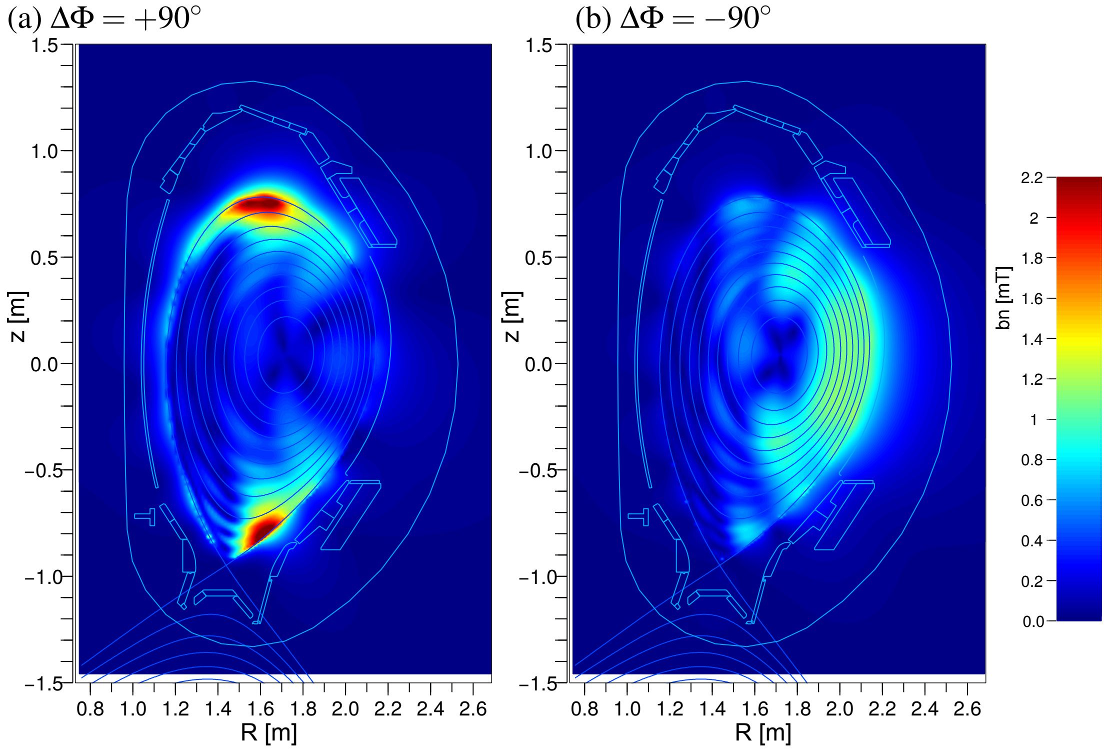

Figure 8. Poloidal distribution of the $n = 2$ plasma response (magnitude of perturbation field normal to unperturbed equilibrium minus non-axisymmetric vacuum field) for (a) $\Delta\Phi = +90°$ and (b) $\Delta\Phi = -90°$

obtained from resistive MHD simulations with MARS-F [81, 61] and JOREK [67] and its reproduction with the NEMEC 3D equilibrium code demonstrates the ideal MHD nature of the field amplification phenomenon.

4. Torque, plasma rotation and field shielding

Torque input and the effect of plasma rotation on field shielding is studied in plasmas with the same low triangularity shape as shown in Fig. 1 but with elevated safety factor $q_{95} = 5.2$ ($B_t = -2.5$ T for central X2 ECRH heating). Figure 9 shows time traces of a discharge where a magnetic perturbation with $n = 1$ is applied with different values of $\Delta\Phi = 45°$ and $\Delta\Phi = 225°$ in successive phases and reference time intervals without MP in between. During a time interval of 200 ms at the end of each MP phase, the plasma is moved towards the MP coils (outer gap reduced) in order to enhance the strength of the MP. One can see that for $\Delta\Phi = 45°$ during this time the ELM frequency increases and the plasma density decreases significantly while no such response is observed for $\Delta\Phi = 225°$.

Fig. 10 shows poloidal mode number spectra for the $n = 1$ component of the vacuum perturbation field for both values of $\Delta\Phi$ at the $q = 2$ and $q = 5$ surface. For $\Delta\Phi = 45°$, the field-aligned resonant component (marked in red) is minimised for the $q = 2$ surface (Fig. 10 a), but not simultaneously for $q = 5$ (Fig. 10 b). Resonant components on surfaces in between have intermediate amplitudes (not shown). This variation is a consequence of the specific

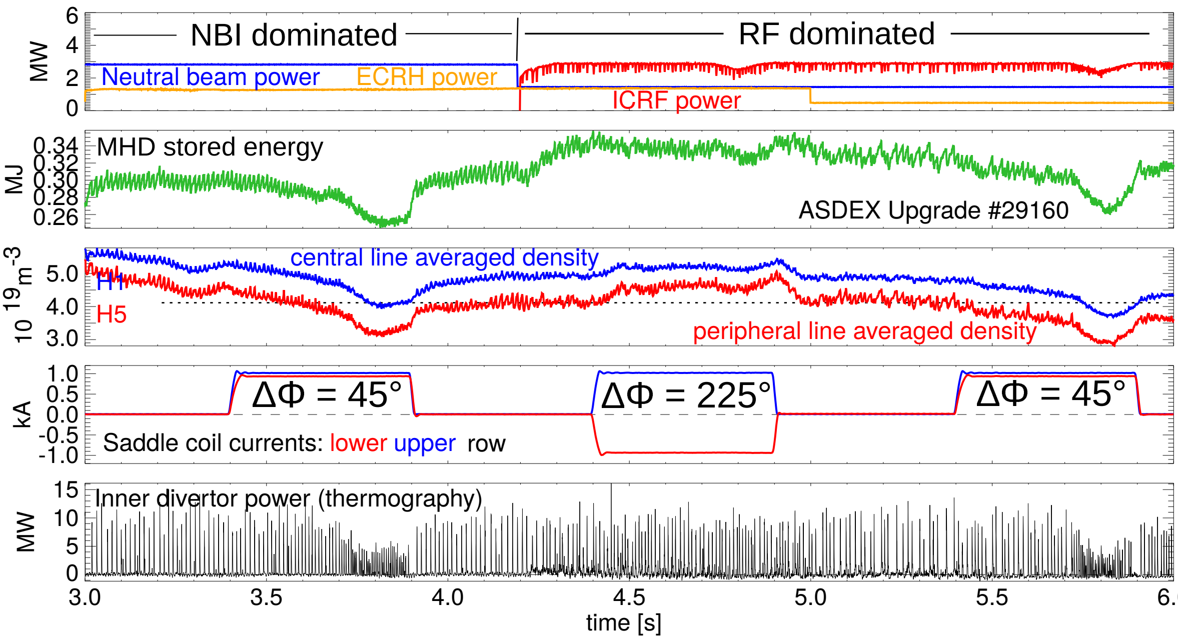

Figure 9. Time traces of shot 29160 with $n = 1$ magnetic perturbations varying the differential phase $\Delta\Phi = 45°, 225°$ and using two different heating schemes (see text).

plasma shape chosen which has finite local shear at the outboard side in between the upper and lower MP coils. Fig. 10 b) also shows that at $q = 5$ ($\Delta\Phi = 45°$) the vacuum spectrum has maxima at $m = 2$ (far from resonance) and $m = 7 = q \cdot n + 2$ (marked in blue). We do not have a plasma response calculation for this case, but in analogy to the discussion in the previous section we conjecture that it is this later component that couples to the edge kink mode and causes the density reduction and ELM mitigation observed in this case. With $\Delta\Phi = 225°$ (differential phase shifted by 180°) the $m = 7$ component is minimised (Fig. 10 d).

We can study now the momentum source introduced by the MP for four different cases: maximum ($\Delta\phi = 45°$) and minimum ($\Delta\phi = 225°$) edge-kink response ($m = qn + 2$), as well as maximum ($\Delta\phi = 315°$) and minimum ($\Delta\phi = 135°$) vacuum resonant response ($m = qn$), This is done by square wave modulation of the MP (Fig. 11). A heating scheme with only $P_{\mathrm{NBI}} = 1.4$ MW and supplementary ICRF heating is chosen to keep the average plasma flow in a range where a strong rotation response of the plasma rotation to the MP is obtained (see below). The time traces in Fig. 11 a) for the case of $\Delta\phi = 45°$ show that both core and edge plasma rotation are clearly affected by the MP modulation, but also density and ELM frequency, albeit to a lower degree. Radial amplitude and phase profiles of the modulated toroidal impurity (boron) rotation measured by charge exchange recombination spectroscopy (CXRS) in response to the MP modulation in the time interval of $t = 4 - 6.5$ s are shown in Fig. 11 b). The phase is relative to the phase of the MP coil current, and increasing values correspond to increasing delay. Only the fundamental frequency at $f = 2$ Hz is considered. One should note that the MP field at the plasma surface at this frequency lags the coil current modulation by 20° (Bu-coils) or 14° (Bl-coils) temporal phase [64]. The radial profiles show that in both cases a minimum of the phase is obtained at the plasma edge. For shot 29344,

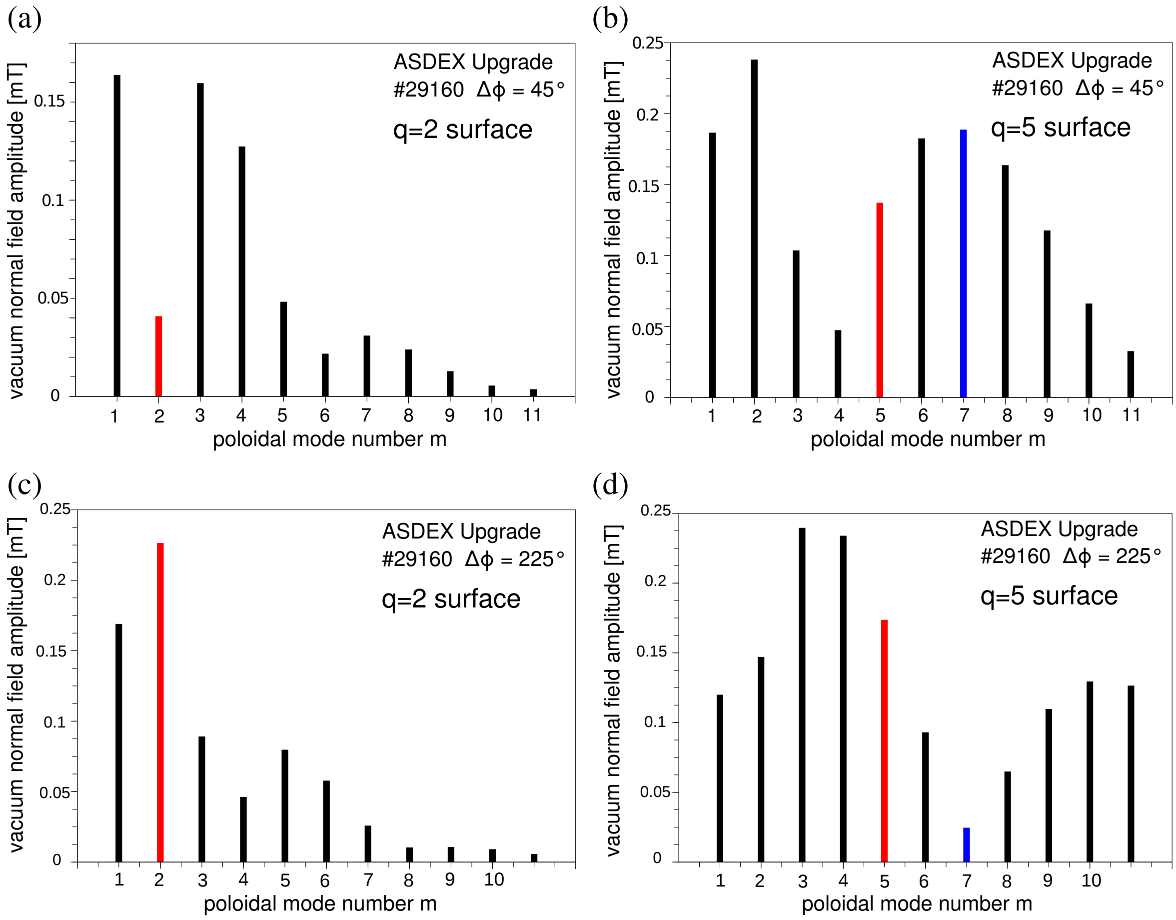

Figure 10. Poloidal mode number spectra for $\Delta\Phi = 45°$ (a,b) and $\Delta\Phi = 225°$ (c,f) for the $q = 2$ (a,c) and $q = 5$ (b,d) surfaces.

at $\Delta\phi = 225°$, the rotation increases slightly with MP on (spin-up), and consequently the phase assumes positive values. The amplitude profile is flat, just above the noise level, and the phase is monotonously increasing from edge to core, suggesting that there is one dominant momentum source at the plasma edge. In all other cases, the rotation decreases with MP on (rotation braking) corresponding to a phase of -180 degrees and above. The phase minimum is again at the plasma edge, however for shot 29342 ($\Delta\Phi = 45°$) the phase flattens inside a normal poloidal flux radius $\rho_{\mathrm{p}} = 0.6$. The amplitude is strongly peaked near the sawtooth inversion radius at $\rho_p = 0.33$ (obtained from electron cyclotron resonance measurements), suggesting that additional torque originates from the interaction with the $m = 1, n = 1$ sawtooth precursor oscillation. Rapid modulation of the sawtooth precursor frequency is observed in ECE measurements. For the cases with maximum ($\Delta\Phi = 315°$) and minimum ($\Delta\Phi = 135°$) vacuum resonant component, rotation braking from the plasma edge is observed like in the case of $\Delta\phi = 45°$ but with smaller amplitudes. The absence of rotation braking (and in fact a spin-up of rotation) only for $\Delta\phi = 225°$ suggests that not the field-aligned resonant component $m = q \cdot n$ governs rotation braking, but the shifted spectral component $m = q \cdot n + 2$ which can excite the edge kink response.

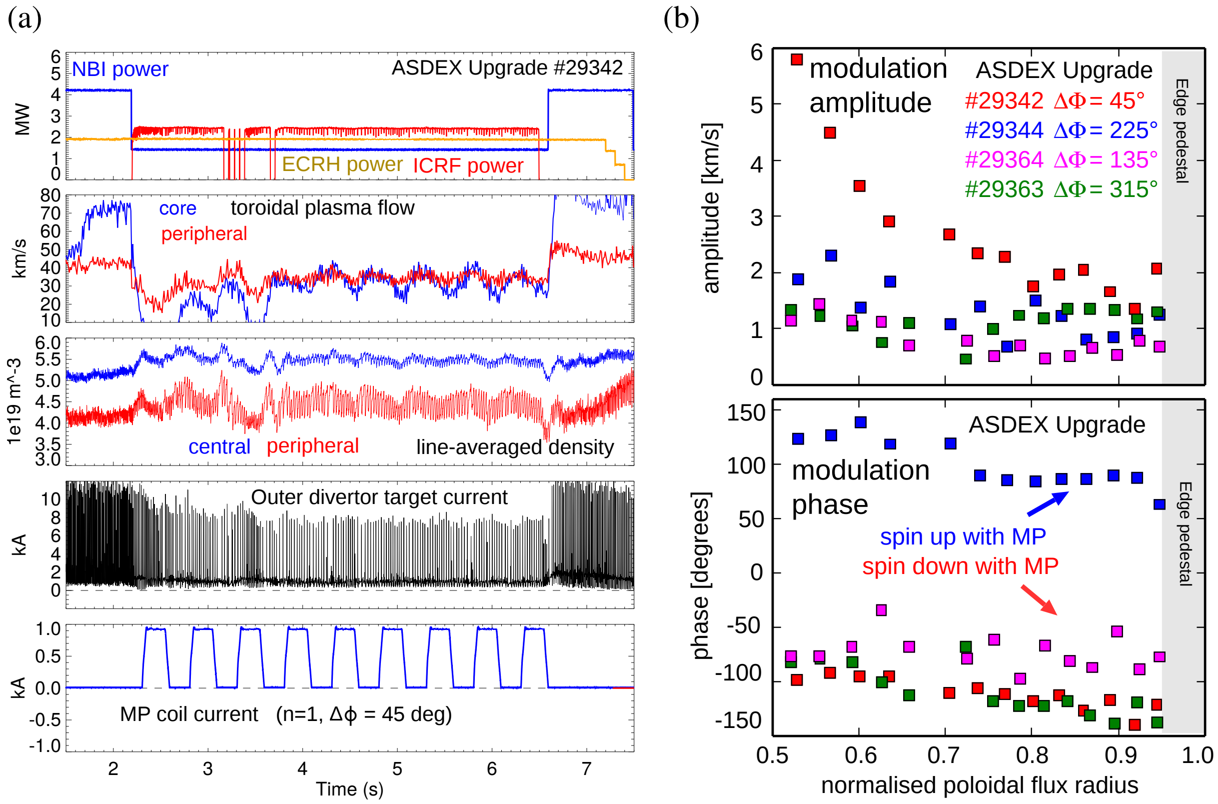

Figure 11. Modulation experiment to find torque deposition radius (a) time traces, (b) amplitude and phase of toroidal boron impurity rotation velocity modulation with $f = 2$ Hz.

The importance of shielding flows is demonstrated in a further experiment, again with $\Delta\phi = 45^\circ$ for maximum plasma response. In shot 29160 (Figure 9) and a series of similar shots the heating mix between NBI, ICRF and ECRH power is varied to vary the plasma co-current rotation velocity while maintaining about constant heating power level of at least 4 MW well above the H-mode threshold which is below 2 MW for these shots. The toroidal rotation velocity of boron impurities, measured again by CXRS, is shown in Fig. 12 (a) for various levels of torque input and MP off or on with $\Delta\phi = 45^\circ$. Rotation braking is strongest for the case of one neutral beam, where the impurity flow slows down to about 20 km/s in co-current direction in the entire plasma. The rotation velocity change is smaller at higher torque, and it is reversed, i.e. causes the impurities to spin up into co-current direction from essentially zero rotation at zero NBI torque (only NBI blips are used for the CXRS measurement). The radial electrical field E_r is obtained from the impurity flow and the impurity diamagnetic velocity using the impurity ion radial force balance. The electron perpendicular flow $v_{e,\perp}$ is then inferred from E_r and the electron diamagnetic velocity using the electron radial force balance. The poloidal impurity flow is not measured over the full profile in this experiment, but substituted by the neoclassical poloidal velocity calculated with NEOART [82, 83]. Previous studies [84, 85] have shown that the poloidal impurity flow in H-mode is essentially neoclassical. It contributes to the radial electrical field mainly in the edge gradient region and is small in the region of flat gradients at the pedestal top. Fig. 12 (b)

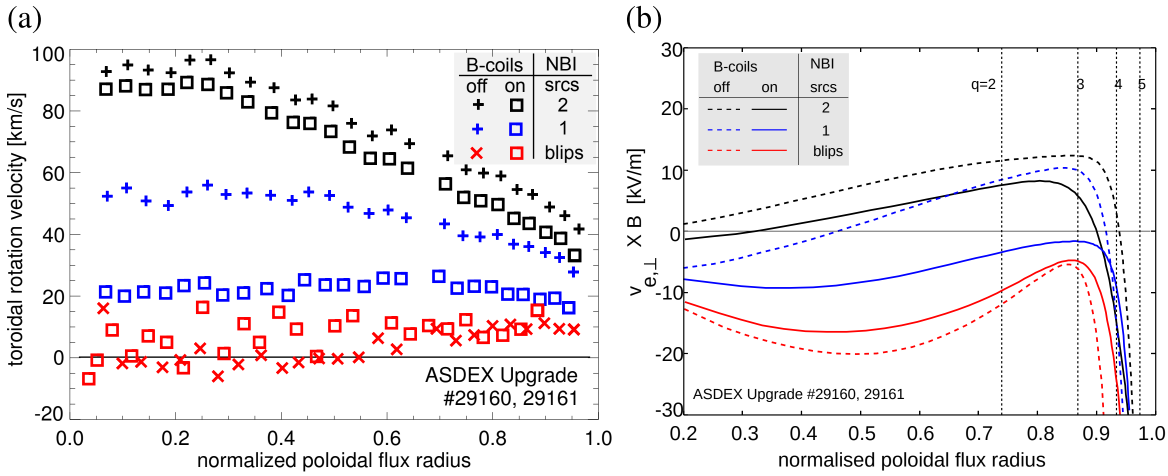

Figure 12. (a) Boron impurity rotation (CXRS at B^{5+}), (b) $v_{e,\perp} \times B$ for $\Delta\phi = 45°$ with and without magnetic perturbations for varying input torque (numbers of NBI sources).

shows $v_{e,\perp} \times B$ for the cases of Fig. 12 (a). For the smallest absolute value of $v_{e,\perp} \times B$ near the $q = 2$ and $q = 3$ surfaces with MP on (blue solid curve), the rotation braking (dashed vs. solid curves) is strongest. Comparing impurity and electron flows, we can conclude that it is the minimum electron perpendicular flow that leads to weakest field shielding and largest plasma response, in agreement with the expected two-fluid nature of the shielding problem.

5. Summary and discussion

5.1. Plasma response in high-confinement mode

We have seen that torque at the plasma edge, near the top of the H-mode edge pedestal, is produced by magnetic perturbations that contain a kink-peeling resonant component and that the torque is towards a direction in which the perpendicular electron flow is reduced. The origin of this torque can be either of resonant or non-resonant nature, and both resonant and non-resonant spectral components are contained in the applied vacuum field and are produced by the plasma response. Non-resonant torque is expected from neoclassical toroidal viscosity (NTV, [86]), however it is predicted to be small in many cases in ASDEX Upgrade compared to neutral beam and resonant torque [87]. NTV torque is caused by non-ambipolarity of radial fluxes and is directed towards restoring ambipolarity. For the ELM mitigation scenario discussed here (shot 31128) the NTV instrinsic rotation is calculated to be in electron direction (inward-directed radial electrical field), because the radial flux of the ions is larger than that of the electrons [86]. In our torque scan experiment, however, the electron perpendicular flow is driven towards zero, independently of whether the initial flow is in ion or electron drift direction on the pedestal top. Resonant torque can be produced by the mode coupling which is intrinsic to kink-peeling amplification of the external perturbation field [61]. The vacuum resonant field is well shielded from rational surfaces on the pedestal top because of the very strong electron flow in the edge gradient region [67]. The maximum resonant response can therefore not be produced by direct coupling to resonant components but only through the kink-peeling amplification mechanism. This appears in our modulation experiment as a shift of poloidal mode number for optimum edge torque by $\Delta m = 2$ with respect to field alignment. If this component is not present in the applied spectrum (but the field-aligned component is) then no rotation braking is observed. Instead, the plasma rotation spins up weakly in ion drift direction. At this stage we can speculate that the spin-up effect might be caused by interaction of the field-aligned MP with the shielding currents in the gradient region where many rational surfaces are closely spaced. The electron perpendicular flow there is strong and in electron direction, while the ion and impurity flows are small and in ion direction so that braking torque on the electrons will cause the ions to spin up.

5.2. ELM mitigation at low pedestal collisionality

We now discuss the implications of our study of plasma response for the ELM mitigation scenario. So far, ELM mitigation has been obtained with a large variation of heating power mix and therefore torque input. In many pulses, $v_{\mathrm{e},\perp}$ crosses zero near the pedestal top but there are also cases in which $v_{\mathrm{e},\perp}$ is negative everywhere and has no zero crossing point. Also there seems to be no limitations in edge safety factor q_{95}. Most of the existing data in ASDEX Upgrade is concentrated around $q_{95} = 3.7$ and $q_{95} = 5.2$ but a few q_{95} ramps have been made and no indication of limited access windows is seen, unlike ELM suppression in DIII-D [43] and ASDEX Upgrade (see below). Also, ELM mitigation is obtained to date with all toroidal mode numbers probed, $n = 1,2,4$, which give rise to differently spaced resonant surfaces. In MAST, the increase of ELM frequency [41] has the same dependence on X-point displacement for different toroidal mode numbers applied [88]. These observations suggests that the number and location of resonant surfaces near the pedestal top are not critical parameters for ELM mitigation. These access criteria are quite different from those to ELM suppression [43].

The mitigating effect on ELMs can still be of resistive nature because of the coupling of modes as predicted in MARS-F [61] and JOREK [67] models. A route for ELM mitigation is suggested [89] based on recent time-dependent resistive JOREK simulations of the non-linear ELM growth with [90] and without [91] presence of MPs. Toroidal coupling of most unstable medium-$n \approx 8$ ELM precursor modes to low-n mode numbers can cause interaction with the applied $n = 2$ MP causing intermediate $n = 4,6$ modes to grow simultaneously which leads in the simulation to small relaxation events before a big ELM is triggered. It may be conjectured that these phenomena correspond to mitigated ELMs in the experiment. To date it is still unclear how this model corresponds to experimental observations. Small type-IV ELMs in MAST have in fact a higher mode number than type-I ELMs [41] and the dominating mode number remains essentially unchanged if type-I ELMs are mitigated in MAST [72]. As yet there is no systematic study on ASDEX Upgrade on this question. It may be noted that toroidal mode coupling is already a feature of ideal MHD and is in fact seen in the NEMEC equilibria described above, because of the full three-dimensional nature of the solution. A finite $n = 4$ perturbation amplitude (not present in the vacuum MP spectrum) appears in the plasma response which originates from mixing of the applied $n = 2$ fundamental with the $n = 6$ aliasing component due to the finite number of eight coils in toroidal direction.

5.3. Prospects for reducing the divertor load due to ELMs

A main concern is the apparent reduction of pedestal pressure in the ELM mitigated regime (Ref. [74] and Fig. 4) which is connected to a confinement reduction compared to the case without MP. Deuterium pellets have been injected [92] to refuel the plasma. While the original plasma density can be restored, the pedestal pressure remains below that without MP due to a reduction of pedestal temperature. Also the ELM losses increase somewhat. Stability analysis for these shots which are of the type of 31128 (low triangularity) shows that the edge is at the peeling-ballooning limit without MP and well stable with MP on both without and with pellet injection [92]. Since there are obviously in all cases individual discernible ELM crash events, one can conjecture that the MP modifies the edge stability limit, which however is below the ideal peeling-ballooning limit of the unperturbed axisymmetric plasma. One may ask whether it is the particle loss related to mitigated ELMs that clamps the density to the reduced level because the ELM frequency increases as the ELM energy loss is reduced. A study of particle losses due to ELMs [93] using a subset of the data of Fig 4 however shows that the ELM particle losses decreases with increasing ELM frequency so that the average particle efflux is essentially independent of the ELM frequency and cannot explain the strong pump-out. One may note that the pump-out effect occurs as well in ELM-suppressed and low density L-mode conditions and therefore does not necessarily rely on the presence of ELMs.

A recent multi-machine scaling study [94] finds that the ELM divertor heat load ε, the areal density of energy deposited by each individual ELM, is essentially proportional to the product of pedestal pressure and the square root of the ELM energy loss, $\varepsilon \propto p_{\text{ped}} \times (\Delta W_{\text{ELM}}/W_{\text{plasma}})^{1/2}$. A small subset of the data contains cases with type-I ELM mitigation by MP in ASDEX Upgrade and this subset has been found in agreement with the scaling [94]. As one can see from Fig. 4, the normalised ELM energy loss from the plasma $\Delta W_{\text{ELM}}/W_{\text{ped}}$ (with $W_{\text{ped}} \propto p_{\text{ped}}$) drops with decreasing density, so the absolute energy loss ΔW_{ELM} drops even faster. If largest and smallest ELM heat losses are compared at fixed pedestal temperature, say $T_e = 1$ keV, $\Delta W_{\text{ELM}}/W_{\text{ped}}$ is reduced by a factor of ≈ 3, accompanied by a density or pressure reduction by a factor of 2. According to the scaling of Ref. [94] and assuming $W_{\text{plasma}} \propto W_{\text{ped}}$, the divertor heat load can expected to be reduced by only a factor $2 \times \sqrt{3} \sim 3.5$ which is smaller than the reduction of ΔW_{ELM} by about a factor of 6. The scaling of Ref. [94] predicts for unmitigated type-I ELM loads in the ITER Q=10 reference scenario a power load of $0.5 - 1.5$ MJ/m^2. Extensive impulsive heat load testing (simulating ELMs) of tungsten monoblocks with realistic numbers of cycles [95] leads to serious microstructural disintegration of the surface above a load of about 0.2 GW/m^2. For an estimated ELM duration of 500 μs in ITER [45], this amounts to 0.1 MJ/m^2, a factor of $5 - 15$ larger than predicted for unmitigated ELMs. It is unclear to date whether the ELM divertor load can be reduced by this factor by means of magnetic perturbations, and whether this can be achieved without unacceptable deterioration of the pedestal pressure. Therefore, scenarios entirely without ELMs and associated divertor heat load transients are an attractive alternative worthwhile to study. A stationary H-mode scenario with full suppression of ELMs has now been established in ASDEX Upgrade and will be studied in detail in further experimentation.

Acknowledgement

This work has been carried out within the framework of the EUROfusion Consortium and has received funding from the Euratom research and training programme 2014-2018 under grant agreement No 633053. The views and opinions expressed herein do not necessarily reflect those of the European Commission.

References

[1] R. Buttery, M. D. Benedetti, D. Gates, Y. Gribov, T. Hender, R. L. Haye, P. Leahy, J. Leuer, A. Morris, A. Santagiustina, et al., Nuclear Fusion 39 (1999) 1827.

[2] S. D. Pinches, I. T. Chapman, P. W. Lauber, H. J. C. Oliver, S. E. Sharapov, K. Shinohara, and K. Tani, Physics of Plasmas 22 (2015).

[3] K. Shinohara, T. Kurki-Suonio, D. Spong, O. Asunta, K. Tani, E. Strumberger, S. Briguglio, T. Koskela, G. Vlad, S. Gnter, et al., Nuclear Fusion 51 (2011) 063028.

[4] J.-K. Park, A. H. Boozer, J. E. Menard, and M. J. Schaffer, Nuclear Fusion 48 (2008) 045006.

[5] I. Barlow, M. Bigi, J. Bird, G. Bonizzoni, R. Buttery, R. Clay, M. D. Benedetti, T. Dobbing, T. Gallagher, G. Gervasini, et al., Fusion Engineering and Design 5859 (2001) 189 .

[6] J. Scoville and R. L. Haye, Nuclear Fusion 43 (2003) 250.

[7] S. M. Wolfe, I. H. Hutchinson, R. S. Granetz, J. Rice, A. Hubbard, A. Lynn, P. Phillips, T. C. Hender, D. F. Howell, R. J. La Haye, et al., Physics of Plasmas 12 (2005).

[8] D. Howell, T. Hender, and G. Cunningham, Nuclear Fusion 47 (2007) 1336.

[9] H. Kim, H. Yang, G. Kim, J.-Y. Kim, H. Jhang, J. Bak, and G. Lee, Fusion Engineering and Design 84 (2009) 1029 , Proceeding of the 25th Symposium on Fusion Technology(SOFT-25).

[10] D. Yao, G. Luo, S. Du, L. Cao, Z. Zhou, T. Xu, X. Ji, C. Liu, C. Liang, Q. Li, et al., Fusion Engineering and Design 9899 (2015) 1692 , Proceedings of the 28th Symposium On Fusion Technology (SOFT-28).

[11] S. S. Abdullaev, T. Eich, and K. H. Finken, Physics of Plasmas 8 (2001).

[12] T. E. Evans, K. H. Burrell, M. E. Fenstermacher, R. A. Moyer, T. H. Osborne, M. J. Schaffer, W. P. West, L. W. Yan, J. A. Boedo, E. J. Doyle, et al., Phys. Plasmas 13 (2006) 56121.

[13] Q. Yu, Physics of Plasmas 13 (2006) 062310.

[14] Q. Yu, Nuclear Fusion 47 (2007) 1244.

[15] P. Ghendrih, M. Bécoulet, L. Colas, A. Grosman, R. Guirlet, J. Gunn, T. Loarer, A. Azroual, V. Basiuk, B. Beaumont, et al., Nuclear Fusion 42 (2002) 1221.

[16] K. H. Finken, S. Abdullaev, W. Biel, M. F. M. de Bock, S. Brezinsek, C. Busch, I. Classen, D. Harting, M. von Hellermann, S. Jachmich, et al., Contributions to Plasma Physics 46 (2006) 515.

[17] E. J. Strait, Physics of Plasmas 22 (2015).

[18] H. Reimerdes, M. S. Chu, A. M. Garofalo, G. L. Jackson, R. J. La Haye, G. A. Navratil, M. Okabayashi, J. T. Scoville, and E. J. Strait, Phys. Rev. Lett. 93 (2004) 135002.

[19] M. Gryaznevich, Y. Liu, T. Hender, D. Howell, M. Beurskens, I. Chapman, C. Challis, E. Joffrin, H. Koslowski, P. Buratti, et al., Nuclear Fusion 52 (2012) 083018.

[20] P. Piovesan, in *Europhysics Conference Abstracts (CD-ROM, Proc. of the 42th EPS Conference on Plasma Physics, Lisbon, Portugal, 2015)*, edited by R. Bingham, W. Suttrop, S. Atzeni, R. Foest, K. McClements, B. Goncalves, C. Silva, and R. Coelho, volume 39E of *ECA*, page P1.144, Geneva, 2015, European Physical Society.

[21] V. Igochine, Nuclear Fusion 52 (2012) 074010.

[22] S. Sabbagh, A. Sontag, J. Bialek, D. Gates, A. Glasser, J. Menard, W. Zhu, M. Bell, R. Bell, A. Bondeson, et al., Nuclear Fusion 46 (2006) 635.

[23] H. Reimerdes, A. M. Garofalo, M. Okabayashi, E. J. Strait, R. Betti, M. S. Chu, B. Hu, Y. In, G. L. Jackson, R. J. L. Haye, et al., Plasma Physics and Controlled Fusion 49 (2007) B349.

[24] P. R. Brunsell, D. Yadikin, D. Gregoratto, R. Paccagnella, Y. Q. Liu, T. Bolzonella, M. Cecconello, J. R. Drake, M. Kuldkepp, G. Manduchi, et al., Plasma Phys. Controlled Fusion 47 (2005) B25.

[25] T. Bolzonella, M. Cavinato, E. Gaio, L. Grando, A. Luchetta, G. Manduchi, G. Marchiori, L. Marrelli, R. Paccagnella, A. Soppelsa, et al., Fusion Engineering and Design 82 (2007) 1064 , Proceedings of the 24th Symposium on Fusion TechnologySOFT-24.

[26] D. F. Escande, P. Martin, S. Ortolani, A. Buffa, P. Franz, L. Marrelli, E. Martines, G. Spizzo, S. Cappello, A. Murari, et al., Phys. Rev. Lett. 85 (2000) 1662.

[27] P. Piovesan, V. Igochine, F. Turco, D. A. Ryan, M. R. Cianciosa, Y. Liu, L. Marrelli, D. Terranova, R. S. Wilcox, A. Wingen, et al., Impact of ideal MHD stability limits on high-beta hybrid operation, EPS

2016 invited paper, submitted to Plasma Phys. Control. Fus.
[28] H. Zohm, Plasma Physics and Controlled Fusion 38 (1996) 105.
[29] K. Kamiya, N. Asakura, J. Boedo, T. Eich, G. Federici, M. Fenstermacher, K. Finken, A. Herrmann, J. Terry, A. kirk, et al., Plasma Physics and Controlled Fusion 49 (2007) S43.
[30] A. W. Leonard, Physics of Plasmas 21 (2014).
[31] P. B. Snyder, H. R. Wilson, T. H. Osborne, and A. W. Leonard, Plasma Physics and Controlled Fusion 46 (2004) A131.
[32] F. Wagner, G. Becker, K. Behringer, D. Campbell, A. Eberhagen, W. Engelhardt, G. Fussmann, O. Gehre, J. Gernhardt, G. v. Gierke, et al., Phys. Rev. Lett. 49 (1982) 1408.
[33] T. SHOJI, H. TAMAI, Y. MIURA, M. MORI, and H. OGAWA, Journal of nuclear materials 196 (1992) 296.
[34] T. C. Hender, R. Fitzpatrick, A. W. Morris, P. G. Carolan, R. D. Durst, T. Edlington, J. Ferreira, S. J. Fielding, P. S. Haynes, J. Hugill, et al., Nucl. Fusion 32 (1992) 2091.
[35] T. Evans, Journal of Nuclear Materials 438, Supplement (2013) S11 , Proceedings of the 20th International Conference on Plasma-Surface Interactions in Controlled Fusion Devices.
[36] Y. Liang, H. R. Koslowski, P. R. Thomas, E. Nardon, B. Alper, P. Andrew, Y. Andrew, G. Arnoux, Y. Baranov, M. Bécoulet, et al., Phys. Rev. Lett. 98 (2007) 265004.
[37] A. Kirk, E. Nardon, R. Akers, M. Bécoulet, G. D. Temmerman, B. Dudson, B. Hnat, Y. Liu, R. Martin, P. Tamain, et al., Nuclear Fusion 50 (2010) 034008.
[38] W. Suttrop, T. Eich, J. C. Fuchs, S. Günter, A. Janzer, A. Herrmann, A. Kallenbach, P. T. Lang, T. Lunt, M. Maraschek, et al., Phys. Rev. Lett. 106 (2011) 225004.
[39] W. Suttrop, L. Barrera, A. Herrmann, R. M. McDermott, T. Eich, R. Fischer, B. Kurzan, P. T. Lang, A. Mlynek, T. Pütterich, et al., Plasma Physics and Controlled Fusion 53 (2011) 124014.
[40] E. Wolfrum, M. Wiesinger, M. Dunne, L. Orte, M. Bernert, R. Fischer, S. Potzel, P. Schneider, W. Suttrop, and ASDEX Upgrade Team, in *Europhysics Conference Abstracts (CD-ROM, Proc. of the 41th EPS Conference on Plasma Physics, Berlin, Germany, 2014)*, edited by S. Ratynskaia, P. Mantica, A. Benuzzi-Mounaix, G. Dilecce, R. Bingham, M. Hirsch, B. Kemnitz, and T. Klinger, volume 38F of *ECA*, page P2.006, Geneva, 2014, European Physical Society.
[41] A. Kirk, W. Suttrop, I. Chapman, Y. Liu, R. Scannell, A. Thornton, L. B. Orte, P. Cahyna, T. Eich, R. Fischer, et al., Nuclear Fusion 55 (2015) 043011.
[42] T. E. Evans, R. A. Moyer, P. R. Thomas, J. G. Watkins, T. H. Osborne, J. A. Boedo, E. J. Doyle, M. E. Fenstermacher, K. H. Finken, R. J. Groebner, et al., Phys. Rev. Lett. 92 (2004) 235003.
[43] T. E. Evans, M. E. Fenstermacher, R. A. Moyer, T. H. Osborne, and J. G. Watkins, Nuclear fusion 48 (2008) 024002.
[44] Y. M. Jeon, J.-K. Park, S. W. Yoon, W. H. Ko, S. G. Lee, K. D. Lee, G. S. Yun, Y. U. Nam, W. C. Kim, J.-G. Kwak, et al., Phys. Rev. Lett. 109 (2012) 035004.
[45] A. Loarte, G. Huijsmans, S. Futatani, L. Baylor, T. Evans, D. M. Orlov, O. Schmitz, M. Bécoulet, P. Cahyna, Y. Gribov, et al., Nuclear Fusion 54 (2014) 033007.
[46] E. Daly, K. Ioki, A. Loarte, A. Martin, A. Brooks, P. Heitzenroeder, M. Kalish, C. Neumeyer, P. Titus, Y. Zhai, et al., Fusion Science and Technology 64 (2013) 168.
[47] M. Jakubowski, S. Abdullaev, K. Finken, and the TEXTOR Team, Nuclear Fusion 44 (2004) S1.
[48] O. Schmitz, T. Evans, M. Fenstermacher, A. McLean, J. Boedo, N. Brooks, H. Frerichs, M. Jakubowski, R. Laengner, C. Lasnier, et al., Journal of Nuclear Materials 415 (2011) S886 , Proceedings of the 19th International Conference on Plasma-Surface Interactions in Controlled Fusion.
[49] A. Wingen, T. E. Evans, and K. H. Spatschek, Physics of Plasmas 18 (2011).
[50] M. Bécoulet, F. Orain, P. Maget, N. Mellet, X. Garbet, E. Nardon, G. Huysmans, T. Casper, A. Loarte, P. Cahyna, et al., Nuclear Fusion 52 (2012) 054003.
[51] P. Cahyna and E. Nardon, Journal of Nuclear Materials 415 (2011) S927 , Proceedings of the 19th International Conference on Plasma-Surface Interactions in Controlled Fusion.
[52] Q. Yu and S. Günter, Nuclear Fusion 51 (2011) 073030.
[53] N. M. Ferraro, Physics of Plasmas 19 (2012).

[54] F. Orain, M. Bécoulet, G. Dif-Pradalier, G. Huijsmans, S. Pamela, E. Nardon, C. Passeron, G. Latu, V. Grandgirard, A. Fil, et al., Physics of Plasmas 20 (2013).

[55] H. R. Koslowski, Y. Liang, A. Krämer-Flecken, K. Löwenbrück, M. von Hellermann, E. Westerhof, R. C. Wolf, O. Zimmermann, and the TEXTOR team, Nucl. Fusion 46 (2006) L1.

[56] W. Suttrop, J. Fuchs, R. Fischer, L. Giannone, A. Herrmann, R. McDermott, M. Maraschek, A. Mlynek, H. Müller, P. Lang, et al., Fusion Engineering and Design 88 (2013) 446 .

[57] Y. Liu, A. Kirk, and E. Nardon, Physics of Plasmas 17 (2010).

[58] R. Fitzpatrick, Plasma Phys. Controlled Fusion 54 (2012) 094002.

[59] Y. Liu, S. Saarelma, M. P. Gryaznevich, T. C. Hender, D. F. Howell, and J.-E. contributors, Plasma Physics and Controlled Fusion 52 (2010) 045011.

[60] Y. Liu, A. Kirk, Y. Gribov, M. Gryaznevich, T. Hender, and E. Nardon, Nuclear Fusion 51 (2011) 083002.

[61] D. A. Ryan, Y. Q. Liu, A. Kirk, W. Suttrop, B. Dudson, M. Dunne, R. Fischer, J. C. Fuchs, M. Garcia-Munoz, B. Kurzan, et al., Plasma Physics and Controlled Fusion 57 (2015) 095008.

[62] C. Paz-Soldan, R. Nazikian, S. R. Haskey, N. C. Logan, E. J. Strait, N. M. Ferraro, J. M. Hanson, J. D. King, M. J. Lanctot, R. A. Moyer, et al., Phys. Rev. Lett. 114 (2015) 105001.

[63] C. Paz-Soldan, N. Logan, S. Haskey, R. Nazikian, E. Strait, X. Chen, N. Ferraro, J. King, B. Lyons, and J.-K. Park, Nuclear Fusion 56 (2016) 056001.

[64] M. Willensdorfer, S. S. Denk, E. Strumberger, W. Suttrop, B. Vanovac, D. Brida, C. M., I. Classen, M. Dunne, S. Fietz, et al., Plasma response measurements of external magnetic perturbations using electron cyclotron emission and comparisons to 3D ideal MHD equilibrium, submitted to Plasma Phys. Control. Fus.

[65] I. Chapman, M. Bécoulet, T. Bird, J. Canik, M. Cianciosa, W. Cooper, T. Evans, N. Ferraro, C. Fuchs, M. Gryaznevich, et al., Nuclear Fusion 54 (2014) 083006.

[66] M. Lanctot, R. Buttery, J. de Grassie, T. Evans, N. Ferraro, J. Hanson, S. Haskey, R. Moyer, R. Nazikian, T. Osborne, et al., Nuclear Fusion 53 (2013) 083019.

[67] F. Orain, M. Hoelzl, E. Viezzer, M. Dunne, M. Bécoulet, G.T.A.Huijsmans, P. Cahyna, J. Morales, M. Willensdorfer, W. Suttrop, et al., Non-linear modeling of the plasma response to RMPs in ASDEX Upgrade, accepted for publication in Nucl. Fus.

[68] W. Suttrop, O. Gruber, S. Günter, D. Hahn, A. Herrmann, M. Rott, T. Vierle, U. Seidel, M. Sempf, B. Streibl, et al., Fusion Engineering and Design 84 (2009) 290.

[69] M. Teschke, N. Arden, H. Eixenberger, M. Rott, and W. Suttrop, Fusion Engineering and Design 9697 (2015) 171 , Proceedings of the 28th Symposium On Fusion Technology (SOFT-28).

[70] H. Höhnle, J. Stober, A. Herrmann, W. Kasparek, F. Leuterer, F. Monaco, R. Neu, D. Schmid-Lorch, H. Schüz, J. Schweinzer, et al., Nuclear Fusion 51 (2011) 083013.

[71] R. Neu, IEEE Transactions on Plasma Science 38 (2010) 453.

[72] A. Kirk, I. T. Chapman, T. E. Evans, C. Ham, J. R. Harrison, G. Huijsmans, Y. Liang, Y. Q. Liu, A. Loarte, W. Suttrop, et al., Plasma Physics and Controlled Fusion 55 (2013) 124003.

[73] I. P. E. G. on Confinement, Transport, I. P. E. G. on Confinement Modelling, Database, and I. P. B. Editors, Nuclear Fusion 39 (1999) 2175.

[74] N. Leuthold, R. Fischer, A. Kappatou, A. Kirk, R. McDermott, A. Mlynek, W. Suttrop, M. Willensdorfer, the ASDEX Upgrade Team, and t. . the EUROfusion MST1 Team.

[75] W. Suttrop, M. Kaufmann, H. J. de Blank, B. Brüsehaber, K. Lackner, V. Mertens, H. Murmann, J. Neuhauser, F. Ryter, H. Salzmann, et al., Plasma Physics and Controlled Fusion 39 (1997) 2051.

[76] T. H. Osborne, R. J. Groebner, L. L. Lao, A. W. Leonard, R. Maingi, R. L. Miller, G. D. Porter, D. M. Thomas, and R. E. Waltz, in *Europhysics Conference Abstracts (Proc. of the 24th EPS Conference on Controlled Fusion and Plasma Physics, Berchtesgaden, 1997)*, edited by M. Schittenhelm, R. Bartiromo, and F. Wagner, volume 21A, part III, pages 1101–1104, Petit-Lancy, 1997, EPS.

[77] R. Sartori, G. Saibene, L. D. Horton, M. Bécoulet, R. Budny, D. Borba, A. Chankin, G. D. Conway, G. Cordey, D. McDonald, et al., Plasma Physics and Controlled Fusion 46 (2004) 723.

[78] A. Kirk, T. O'Gorman, S. Saarelma, R. Scannell, H. R. Wilson, and the MAST team, Plasma Physics and Controlled Fusion 51 (2009) 065016.

[79] E. Strumberger, S. Gnter, P. Merkel, E. Schwarz, C. Tichmann, and H.-P. Zehrfeld, Nuclear Fusion 42 (2002) 827.

[80] E. Strumberger, S. Günter, and C. Tichmann, Nuclear Fusion 54 (2014) 064019.

[81] Y. Liu, D. Ryan, A. Kirk, L. Li, W. Suttrop, M. Dunne, R. Fischer, J. Fuchs, B. Kurzan, P. Piovesan, et al., Nuclear Fusion 56 (2016) 056015.

[82] R. Dux, A. G. Peeters, A. Gude, A. Kallenbach, R. Neu, and ASDEX Upgrade Team, Nuclear Fusion 39 (1999) 1509.

[83] A. G. Peeters, Physics of Plasmas 7 (2000) 268.

[84] E. Viezzer, T. Pütterich, C. Angioni, A. Bergmann, R. Dux, E. Fable, R. McDermott, U. Stroth, E. Wolfrum, and ASDEX Upgrade Team, Nuclear Fusion 54 (2014) 012003.

[85] E. Viezzer, T. Pütterich, R. M. McDermott, G. D. Conway, M. Cavedon, M. G. Dunne, R. Dux, E. Wolfrum, and ASDEX Upgrade Team, Plasma Physics and Controlled Fusion 56 (2014) 075018.

[86] A. F. Martitsch, S. V. Kasilov, W. Kernbichler, G. Kapper, C. G. Albert, M. F. Heyn, H. M. Smith, E. Strumberger, S. Fietz, W. Suttrop, et al., Plasma Physics and Controlled Fusion 58 (2016) 074007.

[87] S. Fietz, A. Bergmann, I. Classen, M. Maraschek, M. Garcia-Muoz, W. Suttrop, H. Zohm, and the ASDEX Upgrade Team, Nuclear Fusion 55 (2015) 013018.

[88] A. Kirk, private communication.

[89] M. Bécoulet, F. Orain, G. T. A. Huijsmans, S. Pamela, P. Cahyna, M. Hoelzl, X. Garbet, E. Franck, E. Sonnendrücker, G. Dif-Pradalier, et al., Phys. Rev. Lett. 113 (2014) 115001.

[90] F. Orain, M. Bécoulet, J. Morales, G. T. A. Huijsmans, G. Dif-Pradalier, M. Hoelzl, X. Garbet, S. Pamela, E. Nardon, C. Passeron, et al., Plasma Physics and Controlled Fusion 57 (2015) 014020.

[91] I. Krebs, M. Hölzl, K. Lackner, and S. Günter, Physics of Plasmas 20 (2013).

[92] M. Valovič, P. Lang, A. Kirk, W. Suttrop, M. Cavedon, G. Cseh, M. Dunne, L. Fischer, L. Garzotti, L. Guimarais, et al., Nuclear Fusion 56 (2016) 066009.

[93] M. Jakubowski et al., Influence of magnetic perturbations on particle transport in magnetic fusion devices, 25th IAEA Int. Conf. on Fusion Energy (St Petersburg, Russia, 2014) EX/P3-47.

[94] T. Eich et al., ELM divertor heat load scaling to ITER with data from JET, MAST and ASDEX Upgrade, PSI 2016, manuscript in preparation.

[95] T. Loewenhoff, J. Linke, G. Pintsuk, R. Pitts, and B. Riccardi, Journal of Nuclear Materials 463 (2015) 202 , PLASMA-SURFACE {INTERACTIONS} 21Proceedings of the 21st International Conference on Plasma-Surface Interactions in Controlled Fusion Devices Kanazawa, Japan May 26-30, 2014.